

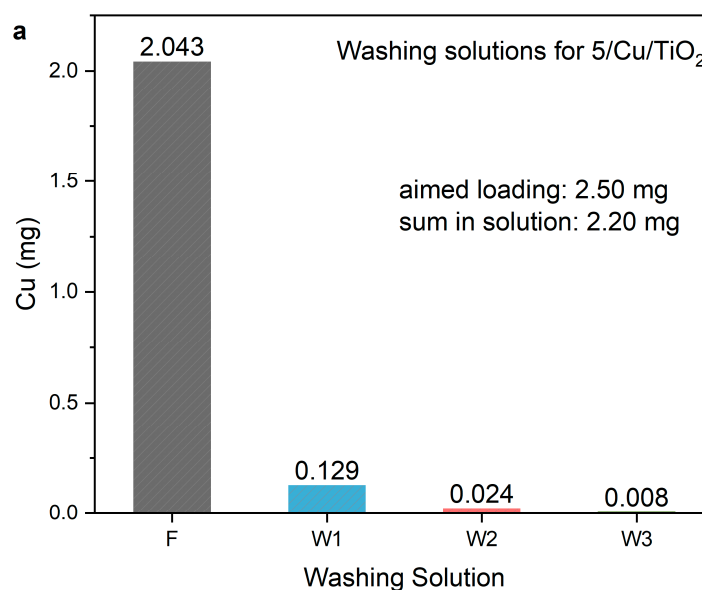
## Supplementary Materials:

# Isolation strategy towards earth-abundant single-site co-catalysts for photocatalytic hydrogen evolution reaction

Pablo Ayala, Ariane Giesriegl, Sreejith P. Nandan, Stephen Nagaraju Myakala, Peter Wobruschek and Alexey Cherevan

### 1. Washing Process

After wet impregnation, the photocatalyst powders were filtered and washed repeatedly. To assure that the impregnated co-catalyst species were stabilized at the surface of  $\text{TiO}_2$  and that a leaching process was not occurring, the liquid solutions were investigated with regard to their elemental composition. As Figure S1 shows, a substantial amount of the precursor species stays in the liquid phase during the impregnation process (especially first filtrate) and further co-catalyst gets washed away afterward in the washing steps. Nevertheless, after the third washing step, the amount of co-catalyst being washed away from the composite materials is negligible. At this point, only the substrate-stabilized co-catalyst species are left at the surface, which determined the number of washing-steps during the synthesis (see Methods).



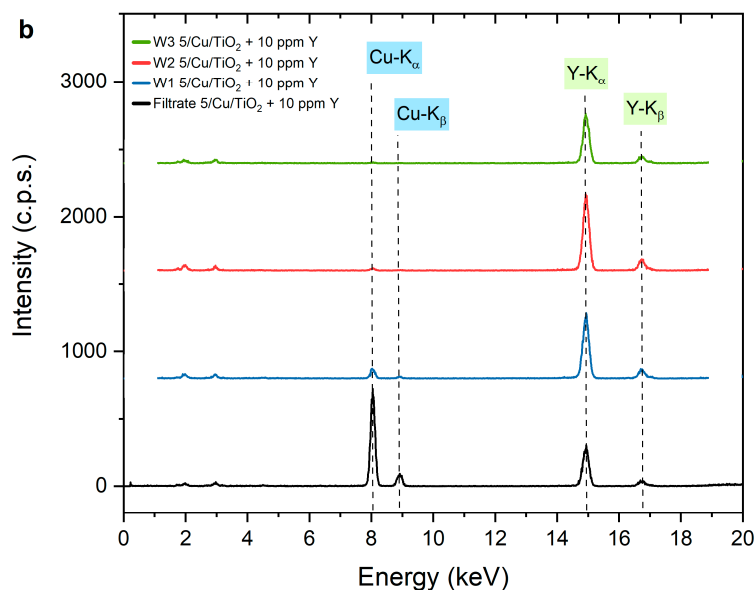


**Figure S1.** Precursor species in liquid solutions after impregnation. (a) Amount of Cu co-catalyst found after impregnation in the filtrate (F) and solutions of the first, second and third washing step (W1-W3). (b) TXRF Spectra of these solutions. Yttrium was used as an internal standard for quantification.

### 1.1. Impact of the precursor

The kind of precursor (i.e. the selected ligands) had a major effect in the co-catalyst loadings of the finished photocatalysts. Figure S2 shows that almost the entire Ni species (99.6 %) added for the impregnation with Ni(Ac)<sub>2</sub> was found in the filtrate. In contrast to this, when Ni(AcAc)<sub>2</sub> was used for impregnation, a reasonably high loading value (similar to that of the comparable Cu(Ac)<sub>2</sub> system) could be achieved.

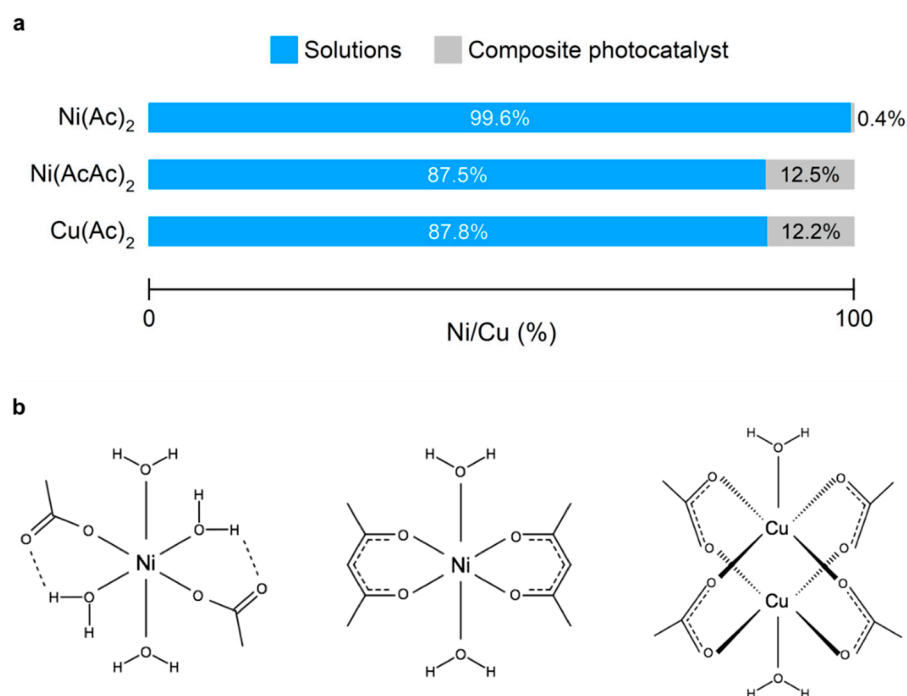


**Figure S2.** Impact of precursor in ultimate loadings. (a) Percentage amounts of the different co-catalyst metals found in the solution (sum of filtrate and washing solutions) and in the composite photocatalysts after impregnation with different metal precursors. Ni acetate showed a decreased adsorption interaction with the support and was washed away easily. Ni acetylacetonate showed a similar loading compared to Cu acetate, which is why it was used for the preparation of the Ni

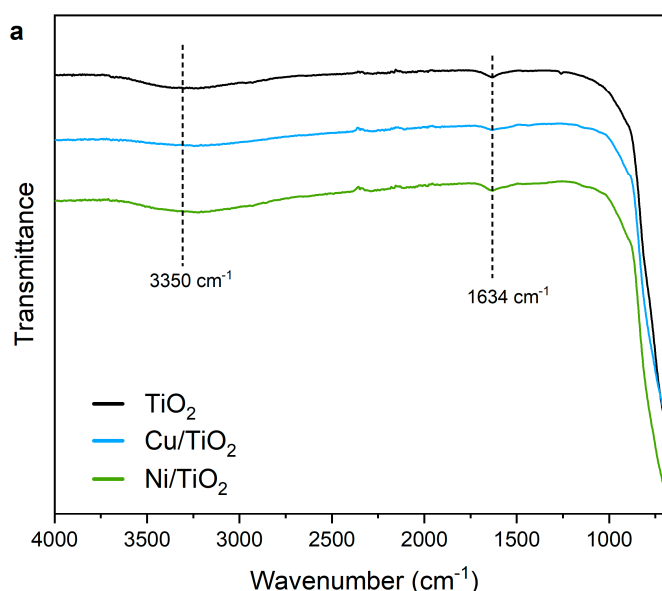
photocatalysts series. (b) Structure of the used precursors:  $\text{Ni}(\text{Ac})_2 \cdot (\text{H}_2\text{O})_4$  (left),  $\text{Ni}(\text{AcAc})_2 \cdot (\text{H}_2\text{O})_2$  (center) and  $\text{Cu}(\text{Ac})_2 \cdot (\text{H}_2\text{O})$  (right).

The explanation to this difference in adsorption is that the complex formed in the aqueous solution of nickel acetate is structurally different from the one formed by nickel acetylacetonate.  $\text{Ni}(\text{AcAc})_2$  is poorly soluble in water due to a stable trimer structure of its anhydrous solid form. In solution, it forms an octahedral complex, with two bidentate bonds from 2 acetylacetonate and 2 aqua ligands, as shown in Figure S2b.  $\text{Ni}(\text{Ac})_2 \cdot 4\text{H}_2\text{O}$ , in turn, is highly soluble in water and forms an octahedral complex as well, but with 4 aqua ligands and only 2 monodentate-bounded acetate ligands [1,2].

We assume that upon adsorption, both complexes anchor to the hydroxylated  $\text{TiO}_2$  surface accompanied by partial ligand exchange. It is important to consider the spectrochemical series that proposes that AcAc is a stronger ligand than Ac, while aqua ligands have an intermediate strength [3]. This suggests that the acetate can be more easily exchanged against an aqua ligand making it more prone to be washed away during the subsequent washing steps. The adsorbed  $\text{Ni}(\text{AcAc})_2$  complex, in comparison, is far less likely to lose its organic ligands so easily during washing due to its higher strength and the additional chelate effect of the bidentate binding. We thus suggest that the AcAc-ligands have a protecting effect against further ligand exchange with aqua-ligands and hence stabilize the adsorbed Ni-species better at the surface of  $\text{TiO}_2$ .

## 2. ATR-FTIR Spectroscopy

To elucidate the Cu and Ni binding modes after impregnation, ATR-FTIR spectra for both prepared photocatalyst's series were taken. Figure S3a shows how the OH-specific ( $3350$  and  $1634 \text{ cm}^{-1}$ ) modes become less pronounced for  $\text{Cu}/\text{TiO}_2$  and  $\text{Ni}/\text{TiO}_2$ , compared to the bare  $\text{TiO}_2$ . However, the  $\text{PO}_4/\text{TiO}_2$  samples do not show such a decrease in intensity for the OH-specific modes, but the  $\text{PO}_4$ -specific modes ( $1048$  and  $1132 \text{ cm}^{-1}$ ) become less pronounced after impregnation.



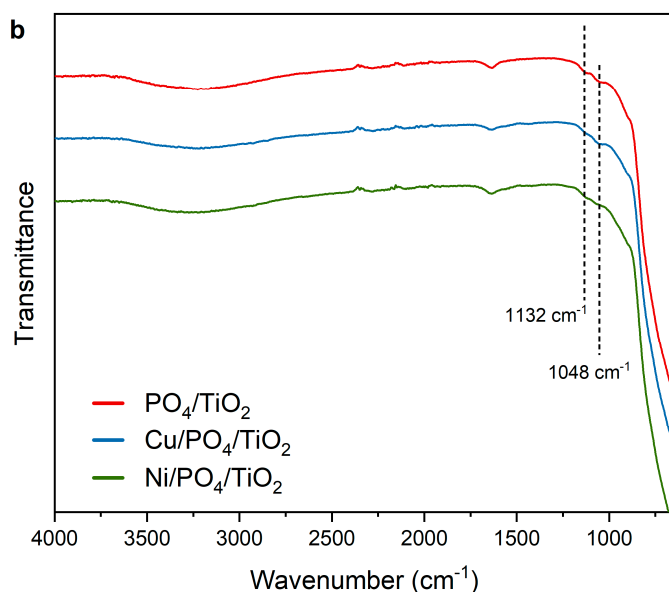


**Figure S3.** ATR-FTIR spectra of the as-prepared photocatalysts in transmittance mode. (a) Bare TiO<sub>2</sub> as a reference and 5/Cu/TiO<sub>2</sub> and 5/Ni/TiO<sub>2</sub> showing a decrease in the OH-specific modes after impregnation. (b) PO<sub>4</sub>/TiO<sub>2</sub> as a reference and 5/Cu/PO<sub>4</sub>/TiO<sub>2</sub> and 5/Ni/PO<sub>4</sub>/TiO<sub>2</sub> showing a decreased intensity in the PO<sub>4</sub>-specific modes after impregnation while the OH-specific modes stay unchanged.

The successful functionalization with phosphate groups at the surface of TiO<sub>2</sub> was confirmed qualitatively through ATR-FTIR. Figure S4 shows the appearance of a shoulder at the region between 1175 and 875 cm<sup>-1</sup> for PO<sub>4</sub>/TiO<sub>2</sub> (red) when compared with bare TiO<sub>2</sub> (black). Upon subtraction of the FTIR data of TiO<sub>2</sub> (dashed inset), the specific modes become clearer, showing specifically at 1132, 1120 and 1048 cm<sup>-1</sup>, all corresponding to phosphorous-oxygen stretching modes in the phosphate anion [4–6].

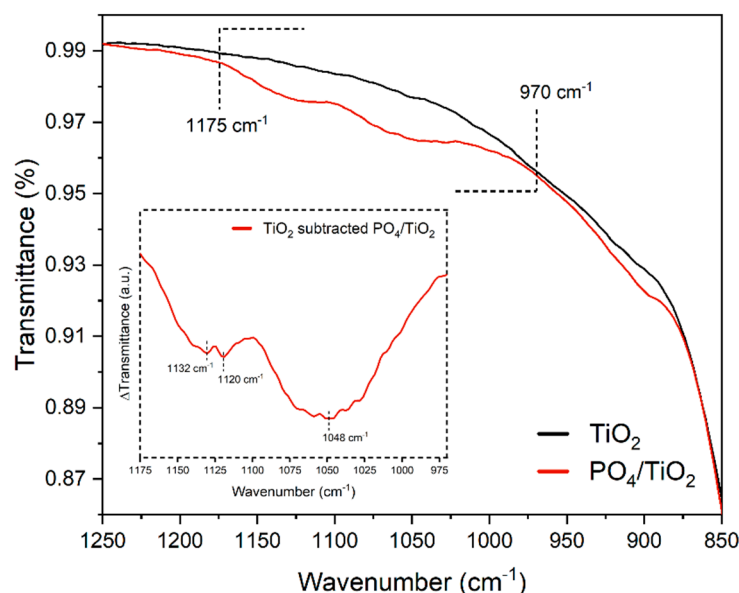


**Figure S4.** ATR-FTIR spectra of the used support materials. PO<sub>4</sub>/TiO<sub>2</sub> (red) shows a characteristic shoulder for this functionalization in comparison to bare TiO<sub>2</sub> (black). The dashed inset shows the enlarged region of interest after subtracting the FTIR data of TiO<sub>2</sub> from the PO<sub>4</sub>/TiO<sub>2</sub> spectrum ( $\Delta$ Transmittance, a.u. = arbitrary units).

### 3. DRS Spectroscopy

DRS-spectra of the Cu and Ni-series on PO<sub>4</sub>/TiO<sub>2</sub> was measured as well to investigate if new features appeared compared to the normal TiO<sub>2</sub>. As seen in Figure S5, no additional

peaks appear, but the existing ones increase in intensity. This is expected, since the PO<sub>4</sub> modification increased the loadings of Cu and Ni, hence, making the modes specific for these co-catalysts more intense.

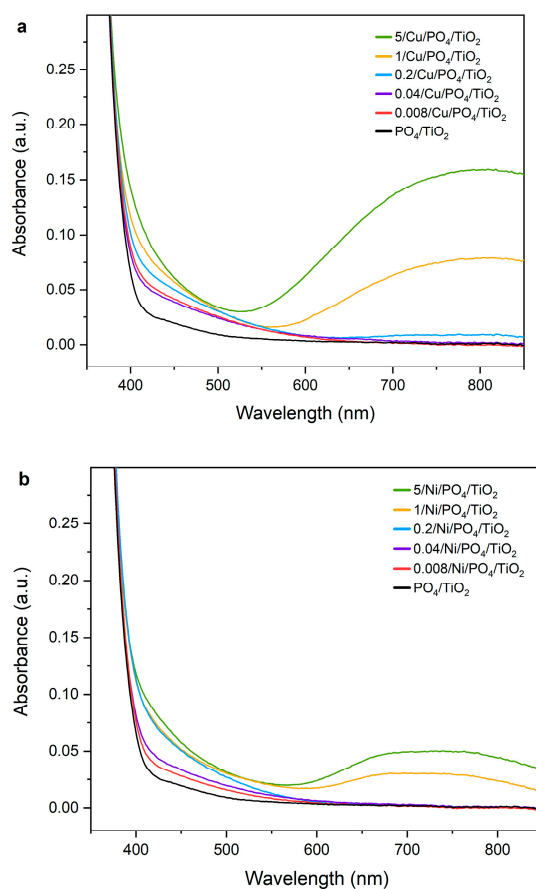


**Figure S5.** Absorbance spectra obtained through DRS measurements of (a) Cu/PO<sub>4</sub>/TiO<sub>2</sub> and (b) Ni/PO<sub>4</sub>/TiO<sub>2</sub> composite series.

#### 4. SEM microscopy

SEM-images acquired for bare TiO<sub>2</sub> and for the Cu/Ni series on this support show no major change in the surface morphology of the photocatalyst before after impregnation, as Figure S6 shows.

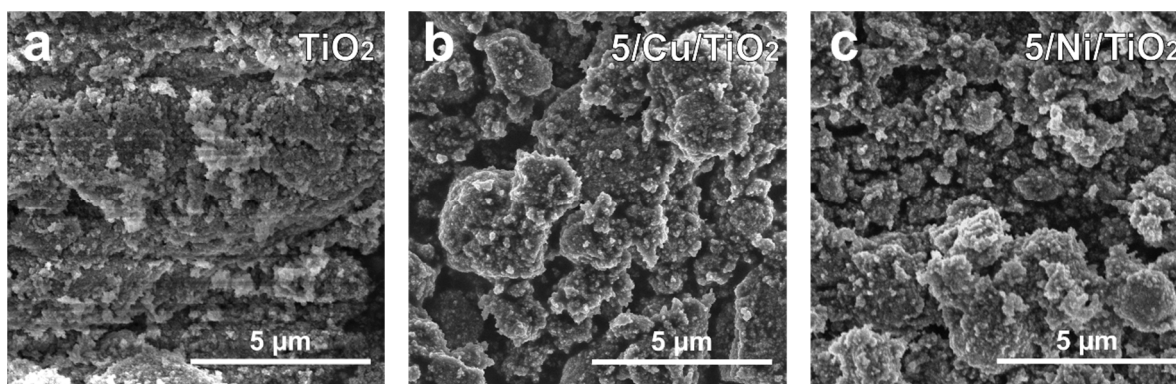


**Figure S6.** SEM-images for morphology comparison on the micron-scale. (a) bare TiO<sub>2</sub>, (b) 5/Cu/TiO<sub>2</sub> and (c) 5/Ni/TiO<sub>2</sub>.

#### 5. HRTEM microscopy

Further TEM-images were acquired to investigate the presence or absence of foreign co-catalyst nanoparticles on the TiO<sub>2</sub> support. As Figure S7 exemplarily shows, no foreign

nanoparticles could be found decorating the Cu and Ni samples on TiO<sub>2</sub> when going towards lower loadings. This was expected for Cu, since no Cu-NPs could be observed at higher loadings (5/Cu/TiO<sub>2</sub>). Ni, in turn, did show Ni-NPs at higher loadings (5/Ni/TiO<sub>2</sub>), suggesting that the isolation strategy (decreasing loadings) does indeed influence the shape/size of the impregnated co-catalyst's clusters, making clusters of Ni/Cu < 1 wt.% irresolvable with the instrument's sensitivity.

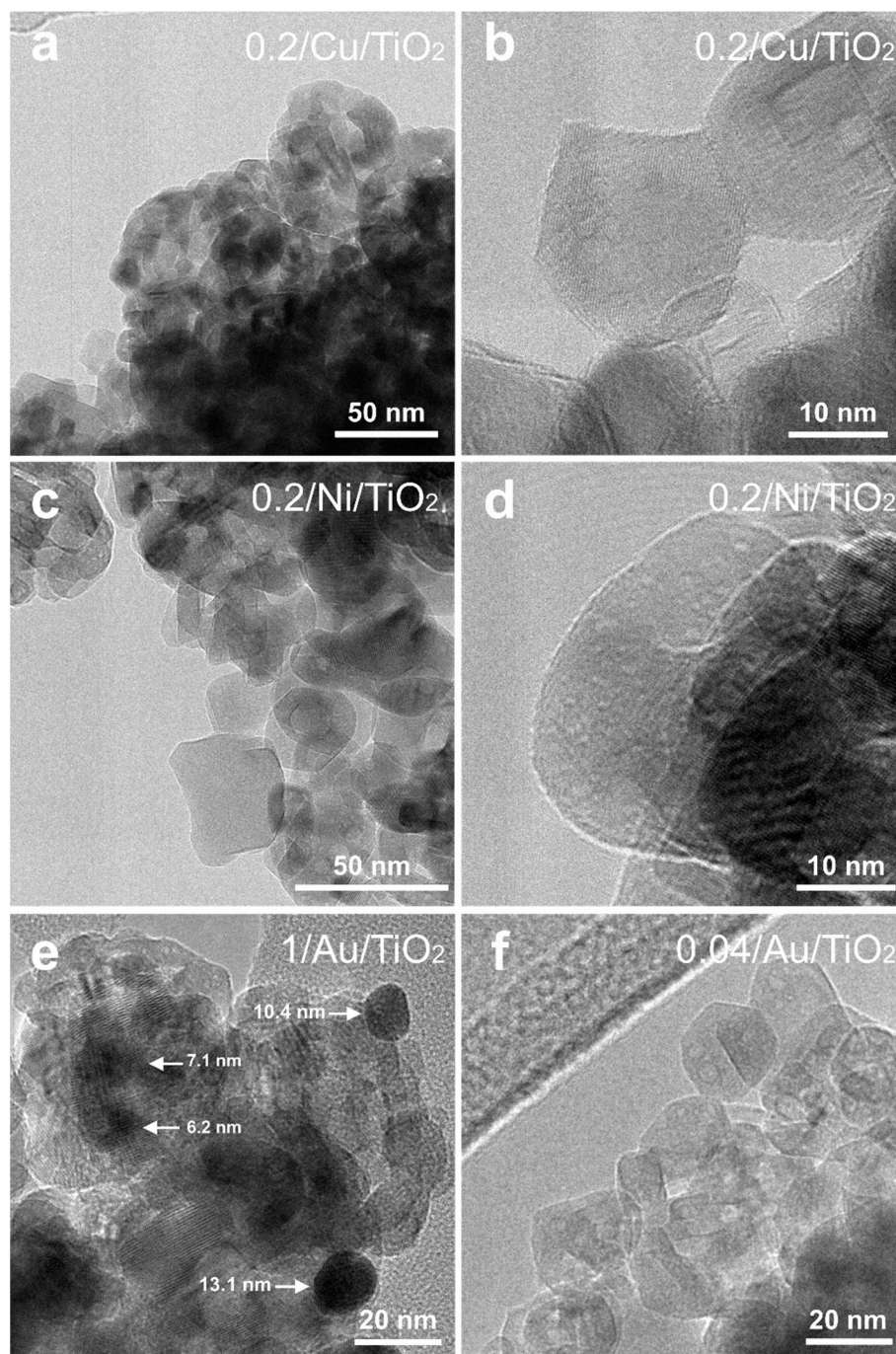


**Figure S7.** TEM-images for the investigation of foreign co-catalyst nanoparticles. Samples with lower intended loadings showing an absolute lack of Cu/Ni nanoparticles for (a, b) 0.2/Cu/TiO<sub>2</sub> at different magnifications and (c, d) 0.2/Ni/TiO<sub>2</sub> at different magnifications. Reference Au-samples on TiO<sub>2</sub> for (e) 1/Au/TiO<sub>2</sub> and (f) 0.04/Au/TiO<sub>2</sub>.

The as-prepared reference Au-samples (see Methods) were also investigated using HRTEM-microscopy. As observed in Figure S6e, the 1/Au/TiO<sub>2</sub> samples show foreign

large Au nanoparticles with a diameter ranging from 6 to 13 nm. Some larger Au nanoparticles were also found occasionally. TEM-images for samples with lower loadings shown in Figure 6Sf (0.04/Au/TiO<sub>2</sub>) do not show any co-catalyst nanoparticles. This further supports the hypothesis that the isolation strategy indeed changes the shape/size of the co-catalyst's clusters upon loading decrease, clearly observed through the disappearance of large Au nanoparticles on the micrographs for the reference Au-samples.

## 6. TOF for reference Au-samples

Following the same synthesis (wet impregnation), characterization (TXRF for real loadings) and HER experiment protocols as described in Methods, the photocatalytic performance of the reference Au-samples was tested. As shown in Figure S8, going towards lower loadings also increases the TOF values and hence the atom utilization efficiency. The relative increase factors of the TOF-values also speak for higher success in the formation of more active species for noble Au on PO<sub>4</sub>/TiO<sub>2</sub> (x10) than on bare TiO<sub>2</sub> (x7) when going from high to low loadings.

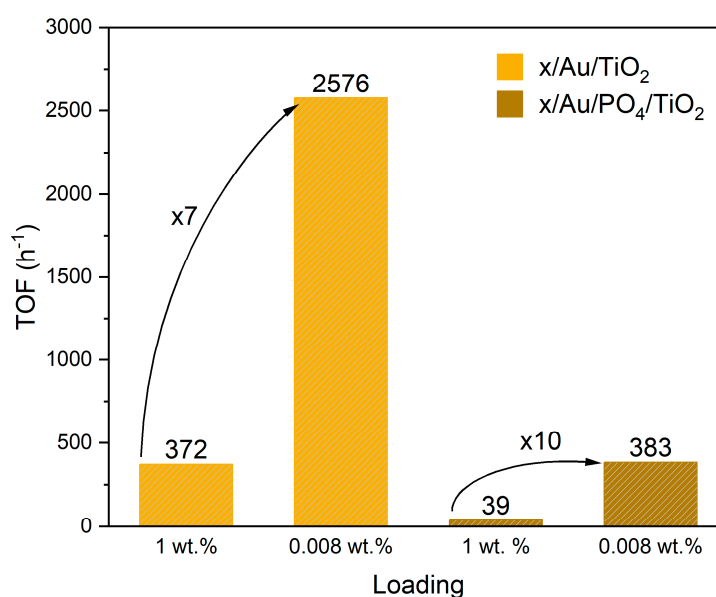


**Figure S8.** TOF values of reference Au-samples against intended loadings for bare TiO<sub>2</sub> (yellow) and PO<sub>4</sub>-modified TiO<sub>2</sub> (ochre). Increase factors are shown with arrows.

## References

- Bullen, G.J.; Mason, R.; Pauling, P. Octahedral Co-Ordination of Nickel in Nickel(II) Bis Acetylacetonate. *Nature* **1961**, *189*, 291–292, doi:10.1038/189291a0.
- Mikuriya, M.; Schumacher, M.; Kawano, C.; Akihara, T.; Ono, K.; Yoshioka, D.; Sakiyama, H.; Handa, M. Dinuclear Nickel(II) Pivalate with M-Aqua and Di-M-Pivalato Bridges Showing a Ferromagnetic Interaction. *ChemJMod* **2014**, *9*, 62–66, doi:10.19261/cjm.2014.09(2).09.
- Atkins, P.; Overton, T. *Shriver and Atkins' Inorganic Chemistry*; OUP Oxford, 2010; ISBN 978-0-19-923617-6.
- Hadjiivanov, K.I.; Klissurski, D.G.; Davydov, A.A. Study of Phosphate-Modified TiO<sub>2</sub> (Anatase). *Journal of Catalysis* **1989**, *116*, 498–505, doi:10.1016/0021-9517(89)90116-4.
- Zhao, D.; Chen, C.; Wang, Y.; Ji, H.; Ma, W.; Zang, L.; Zhao, J. Surface Modification of TiO<sub>2</sub> by Phosphate: Effect on Photocatalytic Activity and Mechanism Implication. *J. Phys. Chem. C* **2008**, *112*, 5993–6001, doi:10.1021/jp712049c.
- Liu, X.; Li, Y.; Peng, S.; Lu, G.; Li, S. Modification of TiO<sub>2</sub> with Sulfate and Phosphate for Enhanced Eosin Y-Sensitized Hydrogen Evolution under Visible Light Illumination. *Photochem. Photobiol. Sci.* **2013**, *12*, 1903–1910, doi:10.1039/C3PP50167A.